Isothermal titration calorimetry with micelles: Thermodynamics of inhibitor binding to carnitine palmitoyltransferase 2 membrane protein☆

Samantha Perspicace[a,1], Arne C. Rufer[b,1], Ralf Thoma[b], Francis Mueller[b], Michael Hennig[b], Simona Ceccarelli[c], Tanja Schulz-Gasch[c], Joachim Seelig[a,*]

[a]Division of Biophysical Chemistry, Biozentrum, University of Basel, CH-4056 Basel, Switzerland
[b]F. Hoffmann-La Roche AG, pRED, Pharma Research & Early Development, Discovery Technologies, Grenzacherstrasse 124, CH 4070 Basel, Switzerland
[c]F. Hoffmann-La Roche AG, pRED, Pharma Research & Early Development, Discovery Chemistry, Grenzacherstrasse 124, CH 4070 Basel, Switzerland

ARTICLE INFO

ABSTRACT

Carnitine palmitoyl transferase 2 (CPT-2) is a key enzyme in the mitochondrial fatty acid metabolism. The active site is comprised of a Y-shaped tunnel with distinct binding sites for the substrate acylcarnitine and the cofactor CoA. We investigated the thermodynamics of binding of four inhibitors directed against either the CoA or the acylcarnitine binding sites using isothermal titration calorimetry (ITC). CPT-2 is a monotopic membrane protein and was solubilized by β-octylglucoside (β-OG) above its critical micellar concentration (CMC) to perform inhibitor titrations in solutions containing detergent micelles. The CMC of β-OG in the presence of inhibitors was measured with ITC and small variations were observed. The inhibitors bound to rat CPT-2 (rCPT-2) with 1:1 stoichiometry and the dissociation constants were in the range of $K_D = 2$–$20\,\mu M$. New X-ray structures and docking models of rCPT-2 in complex with inhibitors enable an analysis of the thermodynamic data in the context of the interaction observed for the individual binding sites of the ligands. For all ligands the binding enthalpy was exothermic, and enthalpy as well as entropy contributed to the binding reaction, with the exception of ST1326 for which binding was solely enthalpy-driven. The substrate analog ST1326 binds to the acylcarnitine binding site and a heat capacity change close to zero suggests a balance of electrostatic and hydrophobic interactions. An excellent correlation of the thermodynamic (ITC) and structural (X-ray crystallography, models) data was observed suggesting that ITC measurements provide valuable information for optimizing inhibitor binding in drug discovery.

© 2013 The Authors. Published by Elsevier B.V. on behalf of Federation of European Biochemical Societies. All rights reserved.

1. Introduction

The carnitine palmitoyltransferase system (CPT) plays an essential role in the β-oxidation of long-chain fatty acids. This transport system consists of three separate proteins. Carnitine palmitoyltransferase 1 (CPT-1), located on the mitochondrial outer membrane, catalyzes the conversion of long-chain fatty acid-CoA esters to acylcarnitine esters [1–3]. Carnitine acylcarnitine translocase (CACT), an integral protein of the mitochondrial inner membrane, facilitates the transport of the acylcarnitine esters from the cytosol into the mitochondrial matrix.

On the luminal side of the mitochondrial inner membrane carnitine palmitoyltransferase 2 (CPT-2) converts the carnitine esters back to CoA esters [4]. Once regenerated, the CoA esters can be oxidized in the β-oxidation pathway. Impaired activity of the CPT-enzymes due to inherited gene mutations is the cause of CPT-deficiency, which can manifest itself in various degrees of clinical severity [2,5]. Metabolic abnormalities of the CPT system may result in different human diseases such as diabetes, obesity or myocardial ischemia and the CPT acyl-carnitine shuttle has hence attracted attention as a target for therapeutic intervention [4,5].

The discovery of a novel class of sulfonamide CPT inhibitors was recently reported [6]. Here, we characterize for selected compounds the binding mode of these inhibitors in comparison to another class of piperidine-based CoA-site binders and also to the established CPT inhibitor ST1326 by calorimetric and crystallographic studies. We focus on interaction with full-length CPT-2 from rat that was expressed in *Escherichia coli* (rCPT-2) because its crystal structure has been solved in contrast to CPT-1, for which no experimental structure of the catalytic domain is available. Solubilization and purification

---

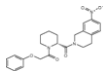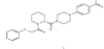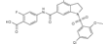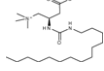1 Contributed equally to this work.
* Corresponding author. Address: Division of Biophysical Chemistry, Biozentrum, University of Basel, Klingelbergstrasse 50/70, CH-4056 Basel, Switzerland. Tel.: +41 61 267 2190; fax: +41 61 267 2189.
   E-mail address: joachim.seelig@unibas.ch (J. Seelig).

Table 1
Molecular weights, structures, IC$_{50}$ values and binding sites for inhibitors 1–4.

	MW (Da)	Structure	IC$_{50}$[a] (μM)	rCPT-2 (binding site)
Inhibitor 1	423.5		2.8	CoA site
Inhibitor 2	449.5		0.15	CoA site
Inhibitor 3	518.9		0.78	CoA site
Inhibitor 4 (ST1326)	399.6		0.38	Acylcarnitine site

[a] IC$_{50}$ values were measured by a spectrophotometric assay as described in Section 2.

of the monotopic membrane protein rCPT-2 in presence of the detergent β-octyl glucoside (β-OG) yielded homogeneous and active enzyme [7,8]. X-ray crytallographic data of rCPT-2 and its complex with the substrate analog and inhibitor ST1326 showed that the active site of the protein is located in a Y shaped tunnel and that this tripartite tunnel comprises binding sites for acyl, carnitine and CoA moieties [7–10]. As rCPT-2 is not soluble in aqueous buffer without addition of detergents, one goal of the present work was to investigate whether isothermal titration calorimetry (ITC) can be used to quantitate the interactions between rCPT-2 and inhibitors in presence of micellar detergent. We previously studied the interaction of a small hydrophobic peptide, cynnamycin, with a phospholipid in buffer that contains β-OG above its critical micellar concentration (CMC) and demonstrated that the binding reaction of the hydrophobic peptide and phospholipid could indeed be measured with ITC [11,12].

In the present study we have first investigated the influence of four different rCPT-2 inhibitors on the CMC of β-OG. Secondly, the binding of the inhibitors to rCPT-2 was measured with ITC in the same micellar environment. The calorimetric titration provided the reaction enthalpy, ΔH^0, and the dissociation constant K_D, from which the changes in free energy, ΔG^0, and entropy, ΔS^0, were calculated. For one inhibitor we also measured the change in heat capacity, ΔC_p^0, by performing ITC experiments at different temperatures, because ΔC_p^0 provides insight into the hydrophobic/hydrophilic balance of inhibitor binding. Finally, we used crystal structures and docking models of rCPT-2 with bound inhibitors for the interpretation of the thermodynamic parameters.

2. Materials and methods

2.1. Protein preparation

Full-length rCPT-2 (658 aa; MW 73.5 kDa) with an amino-terminal His$_6$-tag was expressed in *E. coli* as described [8]. The protein was stored in 25 mM Tris/HCl pH 8, 150 mM NaCl, 2 mM tris-(2-carboxylethyl)-phosphine–HCl (TCEP) supplemented with 1% (w/v) β-OG (~34 mM). Under these conditions rCPT-2 was found to be monomeric and monodisperse, as determined by analytical ultracentrifugation [7]. Variation of the β-OG concentration to lower or higher values caused protein aggregation or competitive binding of β-OG to the acylcanitine site of rCPT-2, respectively. This precluded a titration of the detergent and extrapolation of the binding data to zero β-OG concentration.

2.2. Inhibitors

The structures of inhibitors 1–4 are given in Table 1. Details about the synthesis, structure–activity relationship (SAR) and pharmacology of these compounds are reported in [6].

2.3. Dependency of β-OG critical micellar concentration (CMC) on inhibitor concentration

For ITC experiments the inhibitors were first dissolved in dimethylsulfoxide (DMSO) at a concentration of 10 mM and aliquots of the stock solutions were diluted into the measurement buffer to a final concentration of 100 μM in the presence of 1% DMSO (v/v). Demicellization experiments of β-OG with and without co-dissolved inhibitor were performed with either Omega-ITC or VP-ITC instruments (MicroCal/GE Healthcare, Northampton, MA, USA) using 300 mM β-OG solution containing 1% (v/v) or 7.5% (v/v) DMSO and inhibitors 1–4 at concentrations of 0.75 mM. The solutions were freshly prepared in 25 mM Tris/HCl pH 8, 150 mM NaCl, 2 mM TCEP and were degassed under vacuum for 10 min. The syringe was filled with the micellar β-OG solution and 8 μL aliquots were injected into the calorimeter cell (V_{cell} = 1.4037 ml) containing buffer. During the first few injections the micelles disintegrated completely. The heats of demicellization, δh_i, were recorded and the initial constant δh_i's were used to calculate the heat of demicellization, ΔH_{demic}^0. The heat of micelle formation had the opposite sign, i.e., $\Delta H_{mic}^0 = -\Delta H_{demic}^0$. Depending on temperature, 20–30 injections were needed until the CMC of 23–35 mM was reached in the calorimeter cell and the heat of demicellization approached zero. The demicellization curves were simulated with a cooperative association model [13]. The critical micellar concentration (CMC) was defined as the midpoint of the titration curve [14,15]. The free energy of micellization followed from

$$\Delta G_{mic}^0 = RT \ln \text{CMC} \tag{1}$$

where RT is the thermal energy and the CMC is expressed in molar units.

2.4. Isothermal titration calorimetry (ITC) of inhibitor binding

Binding experiments of rCPT-2 with inhibitors were performed with a VP-ITC calorimeter (V_{cell} = 1.4037 ml; MicroCal/GE Healthcare, Northampton, MA, USA). rCPT-2 was diluted to 10 μM final concentration in 25 mM Tris/HCl pH 8, 150 mM NaCl, 2 mM TCEP, 1% (w/v) β-OG. In order to avoid problems with signal stability during ITC measurements DMSO was also added to the protein solution in the cell at a final concentration of 1% (v/v). The inhibitor solution (ca. 100 μM in buffer with 1% (v/v) DMSO and 1% (w/v) β-OG) was injected in 10 μL steps into a 10 μM rCPT-2 solution in identical buffer. The enthalpy of reaction, ΔH^0, the binding constant, K, and the stoichiometry value, n, were calculated from the measured heat changes, δH_i, upon association of the inhibitor with the rCPT-2 target protein. To examine proton transfer upon binding, titrations with inhibitor 3 were performed in buffers (pH 8) of different ionization enthalpies: HEPES/NaOH (ΔH_{diss} = 3.92 kcal/mol), Bicine/HCl (ΔH_{diss} = 6.27 kcal/mol), Tris/HCl (ΔH_{diss} = 11.52 kcal/mol).

2.5. Measurements of protein stability by thermal unfolding

Differential scanning calorimetry (DSC) measurements for characterization of thermal protein denaturation were performed on a MicroCal VP-DSC calorimeter (V_{cell} = 0.517; MicroCal/GE Healthcare, Northampton, MA, USA). A scan rate of 30 °C/h was used. The protein concentration was 14 μM ($\pm$ 100 μM inhibitor 4) in 25 mM HEPES/NaOH pH 8.0, 150 mM NaCl, 2 mM TCEP and 30 mM β-OG. The reference compartment contained buffer only. A blank measurement with buffer in both compartments was used as baseline. Protein and buffer solutions were degassed to avoid formation of air bubbles.

2.6. Fluorescence quenching experiments

Fluorescence measurements were performed at 20 °C with an SLM-Aminco 8100 double-grating spectrofluorometer. The protein concentration was 2 μM in 25 mM Tris/HCl pH 8, 150 mM NaCl, TCEP

and 1% (w/v) β-OG. The excitation wavelength was 280 nm and protein tryptophan fluorescence was recorded at 340 nm. Small aliquots of known concentration of inhibitors, dissolved in DMSO, were added to the protein solution and each time the fluorescence intensity was measured. These fluorescence intensities were corrected for dilution and ligand absorbance [16], plotted against ligand concentration and fitted for K_D with a single site model as described [17].

2.7. Activity assay

The activity of rCPT-2 (crude lysate from Pichia pastoris expression with 30 nM enzyme concentration) was measured at 30 °C for the reverse reaction with a spectrophotometric assay by using 5-5′-dithiobis-(2-nitrobenzoic acid), DTNB [18,19]. The HS-CoA released on the formation of acylcarnitine from carnitine (500 μM) and palmitoyl-CoA (80 μM) reacted with DTNB (300 mM). The resulting 5-mercapto-(2-nitrobenzoic acid) absorbs at 410 nm with a molar extinction coefficient of $13,600\,M^{-1}\,cm^{-1}$. The assay buffer contained 25 mM Tris–HCl pH 7.4, 120 mM KCl and 1 mM EDTA (and no additional β-OG). Inhibitors 1–4 were titrated from 10 mM DMSO stock solutions. The enzyme activity was not measured in the presence of 1% (w/v) β-OG because in one of the crystal structures a β-OG molecule was bound to the acylcarnitine site (see Supplementary data). β-OG was identified as competitive inhibitor of rCPT-2: with octanoyl-CoA as substrate β-OG had a K_i of 15 mM, which is half the CMC of β-OG [19,20]. In addition, Johnson et al. observed "abnormal non-saturation kinetics with respect to palmitoyl-CoA" (presumably due to self-association of palmitoyl-CoA at high concentrations) [21]. These observations led us to refrain from determining K_i values for inhibitors 1–4.

2.8. X-ray crystallography

rCPT-2 at 12–18 mg/ml was incubated with a 10-fold molar excess of inhibitors (surrogate for inhibitors 1 and 2: [(R)-2-(3,4-dihydro-1H-isoquinoline-2-carbonyl)-peridin-1-yl]-2-phenoxy-ethanone; surrogates for inhibitor 3: 4-{[1-(5-Chloro-2-methoxy-benzenesulfonyl)-4-methyl-2,3-dihydro-1H-indole-6-carbonyl]-amino}-benzoic acid and 2-chloro-4-{[1-(5-chloro-2-methoxy-benzenesulfonyl)-4-methyl-2,3-dihydro-1H-indole-6-carbonyl]-amino}-benzoic acid; see Supplementary Data) and subsequently co-crystallized by vapor diffusion. Crystals for the surrogate of inhibitors 1 and 2 were obtained with 0.1 M bis–Tris pH 6.5, 20% (w/v) PEG–MME 5000 (Index 46, Hampton Research) and 0.05 M magnesium chloride, 0.1 M HEPES pH 7.5, 30% (v/v) PEGMME 550 (Index 55, Hampton Research) and 0.15 M DL-malic acid pH 7.0, 20% (w/v) PEG 3,350 (Index 91, Hampton Research); PEG 200 was used in the cryo-buffer. Crystals for the surrogates of inhibitors 3 were obtained with 0.2 M ammonium sulfate, 0.1 M TRIS/HCl pH 8.5 and 25% (w/v) PEG 3350 (Index 69, Hampton Research) and 0.2 M lithium sulfate, 0.1 M HEPES pH 7.5, 25% (w/v) PEG 3,350 (Index 76, Hampton Research). These crystals were flash frozen in liquid nitrogen after exchanging excess mother liquor against 100% (v/v) paraffin oil. Crystals with inhibitor 4 were obtained as described [8]. Data were collected at 100 K at beamline X10SA of SLS, Villigen, Switzerland, and the crystal structures were solved as described [7,8].

2.9. Binding mode investigation through manual docking of ligands

Manual modeling and energy minimization of inhibitors 1 and 2 was carried out with the modeling package Moloc (Gerber Molecular Design, Basel, Switzerland). The phenoxy moiety of inhibitors 1 and 2 was matched on the phenoxy part of complex structure PDB: 4EYW (inhibitor 1-[(R)-2-(3,4-dihydro-1H-isoquinoline-2-carbonyl)-piperidin-1-yl]-2-phenoxy-ethanone, see Supplementary Data). As in the X-ray complex structure, the phenoxyacetamid part of inhibitors 1 and 2 was modeled in a fully planar conformation to the binding

tunnel. This is a low energy conformation and in agreement with conformational analysis of phenoxyacetyls found in the CSD [22]. In this conformation and orientation in the binding tunnel the phenoxyacetyl carbonyl oxygen is able to form a hydrogen bond to a backbone N–H of Ser490. Flexibility of inhibitors 1 and 2 is limited due the number of ring systems and sp2-centers. This restriction only allows for a conformation where the terminal piperidine/piperazine including fragments bind to an exposed binding pocket. After energy minimization of the ligand with constrained protein atoms the ligands were in an overall low energy conformation with good interactions (hydrogen bonding, VdW) to protein atoms.

3. Results

3.1. Thermodynamics of micelle formation

The chemical structure of the inhibitors investigated is given in Table 1. Fig. 1 summarizes the influence of DMSO and inhibitors 1–4 on the critical micellar concentration (CMC) of β-OG. Fig. 1A displays the critical CMC of β-OG in buffer with and without addition of DMSO as a function of temperature. The data in absence of DMSO are very similar to those of previous reports [15,23]. Addition of 1% (v/v) DMSO shifts the CMC to higher values by about 2–3 mM, and increasing the concentration of DMSO to 7.5% (v/v) has an even larger effect with a 6–8 mM increase of the CMC. The addition of DMSO shields hydrophobic interactions of detergent molecules and thus makes micelle formation more difficult, which results in an increase of the CMC.

Fig. 1B compares micelle formation upon addition of inhibitors 1–4. The starting solution of the demicellization experiment was typically 300 mM β-OG with 0.75 mM inhibitor and 7.5% (v/v) DMSO. Diluting this solution to 40 mM β-OG produces an inhibitor concentration of 100 μM. This corresponds approximately to the standard solution used in the protein binding experiments. Inspection of Fig. 1B reveals different inhibitor effects on the CMC. The presence of inhibitor 3 has no effect on the CMC of β-OG when compared to β-OG alone. Inhibitors 2 and 4 slightly increase the CMC of β-OG. In contrast, inhibitor 1 reverses completely the effect of 7.5% DMSO and the CMC becomes close to that of pure β-OG without DMSO. The only difference between inhibitors 1 and 2 is the polar nitro-group of inhibitor 1, which could have a specific interaction with DMSO.

Fig. 1C summarizes the temperature dependence of the enthalpy of micelle formation, ΔH^0_{mic}. From the slopes of the linear fits the molar heat capacity change of micelle formation can be calculated as $\Delta C^0_p = -60$ to -90 cal/mol K, which is typical for a hydrophobic aggregation reaction of molecules of the size of β-OG. Van't Hoff's law was used to calculate the temperature dependence of the CMC as shown by the solid lines in Fig. 1A and B. All thermodynamic data are summarized in Table 2. As a general conclusion it follows that the addition of DMSO or inhibitors 1–4 has a small influence on the CMC of β-OG but does not induce significant changes of micelle structure or micelle–solvent interactions.

3.2. Inhibitor binding to rCPT-2 measured by isothermal titration calorimetry

Inhibitors were dissolved in micellar β-OG at concentrations of 100–300 μM and were titrated into 10 μM rCPT-2. A typical titration experiment is shown in Fig. 2A. After an initial exothermic reaction the heats of reaction reached a constant value. The heat flows were integrated to yield the heats of reaction, δh_i, (Fig. 2B). The heat of dilution towards the end of the reaction was subtracted before evaluating the data. The solid line in Fig. 2B corresponds to a binding model with a 1:1 stoichiometry and was calculated with $\Delta H^0 = -4.7$ kcal/mol and a binding constant $K = 8 \times 10^5\,M^{-1}$.

Table 3 summarizes the thermodynamic data derived from ITC measurements. The dissociation constants $K_D = 1/K$ determined by

Table 2
Effect of inhibitors 1–4 on micelle formation of β-OG (values measured in absence of rCPT-2).

	Temp. (°C)	CMC (mM)	ΔH_{mic}^0 (kcal/mol)	ΔG_{mic}^0 (kcal/mol)	$T\Delta S_{mic}^0$ (kcal/mol)
β-OG + no inhibitor					
	14	32.8	1.33	−1.94	3.27
	30	27.8	0.60	−2.15	2.75
	37	28.6	0.16	−2.18	2.34
	45	–	−0.54	–	–
β-OG + inhibitor 1					
	14	24.1	1.24	−2.12	3.36
	25	23.3	0.30	−2.22	2.51
	37	24.1	−0.88	−2.29	1.40
β-OG + inhibitor 2					
	14	34.5	1.03	−1.91	2.94
	45	33.3	−0.74	−2.14	1.40
β-OG + inhibitor 3					
	14	32.3	1.28	−1.95	3.23
	45	29.0	−0.59	−2.23	1.64
β-OG + inhibitor 4					
	14	35.1	2.36	−1.90	3.26
	25	31.3	0.88	−2.04	2.92
	30	31.0	0.57	−2.08	2.66
	45	31.0	−0.45	−2.19	1.74

ITC are supported by the results of fluorescence titrations, which yielded similar affinities for inhibitors 1–3. The binding reactions of all four inhibitors followed a 1:1 stoichiometry. Inhibitors 1, 2 and 4 showed exothermic reaction enthalpies in Tris/HCl pH 8 buffer while the reaction of inhibitor 3 was endothermic under the same conditions.

The interaction of inhibitors 1 and 2, which according to our models bind to the CoA-site of rCPT-2 (Fig. 3), was driven to almost equal extent by enthalpy and entropy. Inhibitor 4 to binds to the acylcarnitine binding site of rCPT-2 and this interaction was enthalpy driven. The entropy term even counteracted the binding because the conformational flexibility of the acyl-moiety is frozen upon binding. For inhibitor 3, which – according to our crystal structures and docking models – binds to the CoA binding site but with a different binding mode than inhibitors 1 and 2, binding to rCPT-2 appeared to be purely entropy-driven in Tris/HCl pH 8.0. Among the tested compounds inhibitor 3 was the only molecule which carried a carboxylic acid group. Inspection of the crystal structure of rCPT-2 in complex with inhibitor 3 shows the carboxy-group at a distance of ~2.8Å from the side chain of the catalytic His372 (Fig. 3), suggesting that the endothermic ΔH could have been caused by a proton transfer (see paragraph on protonation reaction below). This is supported by our observation that a change to buffers with different dissociation enthalpies led to exothermic binding reactions for this compound.

3.3. Protonation reaction

Inhibitor 3 carries a carboxylic acid group with a calculated pK_a = 3.5 [24,25], which is deprotonated in the Tris/HCl pH 8 buffer. To investigate whether proton transfer can occur between the carboxylic acid group and the catalytic His372, we have measured the binding of inhibitor 3 to rCPT-2 at pH 8 in buffers with different dissociation enthalpies (25 mM HEPES/NaOH, $\Delta H_{diss} = 3.92$ and 25 mM Bicine/NaOH, $\Delta H_{diss} = 6.28$). The measured reaction enthalpy, ΔH_{obs}, is composed of the intrinsic binding enthalpy, ΔH_1, of inhibitor 3 to rCPT-2 plus the additional enthalpies of inhibitor protonation, ΔH_2, and buffer dissociation, ΔH_{diss}.

$$\Delta H_{obs} = \Delta H_1 + n(\Delta H_{diss} - \Delta H_2) \qquad (2)$$

where n is the number of protons transferred from buffer to inhibitor. In Fig. 4 the measured ΔH_{obs} is plotted versus the dissociation enthalpies of 3 different buffers. A straight line with $n = 0.83 \pm 0.17$ is obtained, indicating that the binding of inhibitor 3 to rCPT-2 induces

a protonation of inhibitor 3 by 0.8 H^+. The intercept with the ordinate is $\Delta H_1 - n\Delta H_2 = -7.14$ kcal/mol. As the dissociation enthalpy of acetic acid is $\Delta H_2 = -0.1$ kcal/mol [26] and assuming the same value for the carboxylate group of inhibitor 3 we find an intrinsic binding enthalpy of $\Delta H_1 = -7.8 \pm 1.3$ kcal/mol for inhibitor 3. The binding of inhibitor 3 to the CoA site is thus driven by a change in enthalpy, suggesting strong van-der-Waals interactions.

3.4. Protein stability and ligand binding

We used differential scanning calorimetry (DSC) to investigate to which extent ligand binding could stabilize the protein structure. We measured the thermal unfolding of rCPT-2 both in absence and presence of inhibitor 4 (Fig. 5). In both experiments a plot of C_p^0 versus temperature showed a broad, asymmetric transition, extending from 30 to 55 °C. The midpoints of the transition were at 47.2 °C for the pure protein and at 49.8 °C for rCPT-2 bound with inhibitor 4. The midpoint of unfolding as seen by DSC for the protein without inhibitor is in good agreement with a fluorescent-based thermal shift assay and circular dichroism spectroscopy which determined melting points as $T_m = 47.6$ °C and 47.0 °C, respectively [7]. The integration of the C_p^0 versus temperature curve in the interval 30–55 °C yields a total unfolding enthalpy of 970 kcal/mol for the protein without inhibitor and 1270 kcal/mol for the protein in excess of inhibitor 4. The rCPT-2 unfolding does not follow a simple N(ative) $\rightleftharpoons$ U(nfolded) 2-state transition. Nevertheless, it can be estimated that the observed stability increases of ~3 °C together with the measured ΔH-values leads to a binding constant in broad agreement with that observed by ITC.

4. Discussion

rCPT-2 is a 658 amino acid peripheral membrane protein which is located at the matrix side of the inner mitochondrial membrane. It belongs to a class of enzymes where both hydrophobic and hydrophilic interactions are important. Potential mechanisms to overcome the phospholipid/water boundaries have been reviewed [27]. Based on the crystal structure of rCPT-2 it was suggested that two helices with hydrophobic residues are submerged by 4–5 Å into the core of the membrane [7]. The present study explored the potential to perform thermodynamic binding studies in the micellar detergent environment necessary for solubilization of active rCPT-2. It was expected that hydrophobic interactions were reduced in a non-polar environment whereas electrostatic interactions were increased due to the

Table 3
Results of **A**, ITC and **B**, fluorescence as well as activity measurements for inhibitors 1–4. See Section 2 for IC$_{50}$ and minimum/maximum K_i values.

A

Inhibitor	T (°C)	K_D (µM)	ΔG^0 (kcal/mol)	ΔH^0 (kcal/mol)	TΔS^0 (kcal/mol)	Comment
1	10	1.6 ± 0.4	−7.5 ± 0.1	−3.9 ± 0.9	3.7 ± 0.8	Average ± SEM of two replicates
	17	6.6	−6.8	−1.6	5.2	–
2	10	2.0	−7.4	−3.0	4.4	–
	17	2.0	−7.5	−5	5.0	–
3	10	5.0	−6.8	−5.0	1.8	25 mM HEPES/NaOH pH 8 (ΔH_{diss} = 3.92 kcal/mol)
	10	5.0	−6.8	−1.8	5.0	25 mM Bicine/NaOH pH 8 (ΔH_{diss} = 6.28 kcal/mol)
	10	3.3	−7.1	1.6	8.7	ΔC_P^0 = 69 cal mol^{-1} K^{-1}
	17	3.5	−7.2	2.2	9.4	
	25	2.9	−7.5	2.6	10.1	
	37	5.0	−7.5	3.5	11	
4	10	10.5 ± 3.3	−6.5 ± 0.3	−9.8 ± 0.7	−3.3 ± 0.5	Average ± SEM of three replicates
	37	20.0	−5.9	−9.5	−3.7	–

B

Inhibitor	K_D (µM)	IC$_{50}$ (µM)
	Fluorescence (20 °C)	Diluted lysate (30 °C)
1	16.2	2.8
2	15.5	0.15
3	5.2	0.78
4	n.d.	0.38

lower dielectric constant of the solvent. So far, there is only limited calorimetric data available for ligands binding to detergent solubilized membrane proteins [28,29], or the interaction of small molecules or peptides with phospholipids [11,12].

Fig. 3 shows the superposition of inhibitors 1–4 (or analogs thereof, see Supplementary Data) on the rCPT-2 active site. Inhibitors 1–3 bind to the CoA binding site, while inhibitor 4 (ST1326) binds to the acyl-carnitine site. Two different modes of interaction were found for CoA site binders. The piperidine derivatives (inhibitors 1 and 2) interact with residues of β-strand 13 (Ser490) and a pocket created by the subsequent loop (Ala492, Ala493) and β-strand 2 (Phe176). Inhibitor 3 of the sulfonamide class interacts directly with the catalytic His372 via its carboxy-group as well as with residues of the loop that connects β-strands 15 and 16 (Thr 591, Leu 592, Asn 593). In the presence of inhibitors of the sulfonamide class the peptide bond between Asp376 and Gly377 adopts a conformation such that the amide nitrogen atom of Gly377 points towards the carboxyl-group of the inhibitors. Thereby a hydrogen-bond network between the catalytic loop (Glu371–Gly377) and the inhibitor is established, for which direct evidence is provided by the protonation of the inhibitor carboxy-group observed in the ITC experiments. We have previously recognized the peptide flip between residues Asp376 and Gly377 and its potential utilization as anchor-point for CPT inhibitors targeted against the CoA site [7]. With inhibitor 3 of the sulfonamide class of CPT-2 inhibitors we provide a first example. In the case of inhibitor 4, the C14 alkyl-chain occupies an essentially hydrophobic tunnel spanning from the active site of the protein to its surface [7], while the hydrophilic carnitine head-group is bound in a hydrogen network comprising residues of the catalytic loop, α-helix 5 (Tyr120) and β-strands 15 and 16 and an additional cation-π interaction with Phe602. The reduction of the conformational flexibility of the alkyl-chain and the formation of the hydrogen network upon binding of ST1326 to rCPT-2 explains both the negative entropy and the large exothermic enthalpy of the binding reaction observed in ITC experiments.

In the present study we investigated which thermodynamic forces govern the interaction between rCPT-2 and its substrates. Isothermal titration calorimetry measures the reaction enthalpy, ΔH^0, but also provides the dissociation constant K_D from the shape of the titration curve. The dissociation constants determined by ITC are in the range of 2 µM (inhibitor 1) to 20 µM (inhibitor 4) and values of the same order of magnitude were measured with fluorescence titrations. The differences in K_D values between ITC and fluorescence spectroscopy must be attributed to the different assay conditions. In addition, β-OG can bind to the acylcarnitine binding site of rCPT-2 and inhibit its activity (see Section 2 and Supplementary data). When compared to the ITC experiments, lower protein concentrations have to be used and the inhibitors are added from DMSO stock solutions for our standard fluorescence spectroscopy protocol. A lower ratio of rCPT-2 to β-OG and thus a higher fraction of β-OG micelles without rCPT-2 insertion could reduce the apparent affinity of the inhibitors for rCPT-2 in the fluorescence titrations, especially with regard to partition of inhibitors 1 and 2 into β-OG micelles (Fig. 1, Table 2). Along these lines, the similar K_D values of the ITC and fluorescence titration results in the case of inhibitor 3 agrees with the observation that inhibitor 3 had no effect on the CMC of β-OG.

In contrast to the binding assays the enzymatic activity measurements were made with diluted rCPT-2 extracts without additional detergent and, thus, the hydrophobic solvent effects were strong. The non-polar reaction partners were hydrated and water molecules were released upon binding, leading to a strong positive entropy contribution to binding. In contrast, 1% (w/v) β-OG was used in the ITC experiments and consequently rCPT-2 and the inhibitors were already embedded in a hydrophobic, micellar environment and the molecules were hydrated to lesser extent. The hydrophobic effect was accordingly reduced. The solvent effect was particularly pronounced for inhibitor 4 which carries a C14 aliphatic chain. In the aqueous phase the hydrophobic effect of this residue was dominant, whereas the hydrophobic effect was essentially eliminated in the presence of micellar β-OG and the entropy contribution became negative.

As mentioned in Section 1, the binding of cynnamycin, a 19 aa tetra-cyclic peptide, to phospholipids with the phosphoethanolamine (PE) headgroup was compared in water and in micellar phase [11,12]. The free energy of binding, ΔG^0, was by 1–2.5 kcal/mol less negative in β-OG micelles than in the aqueous phase. The binding constants of
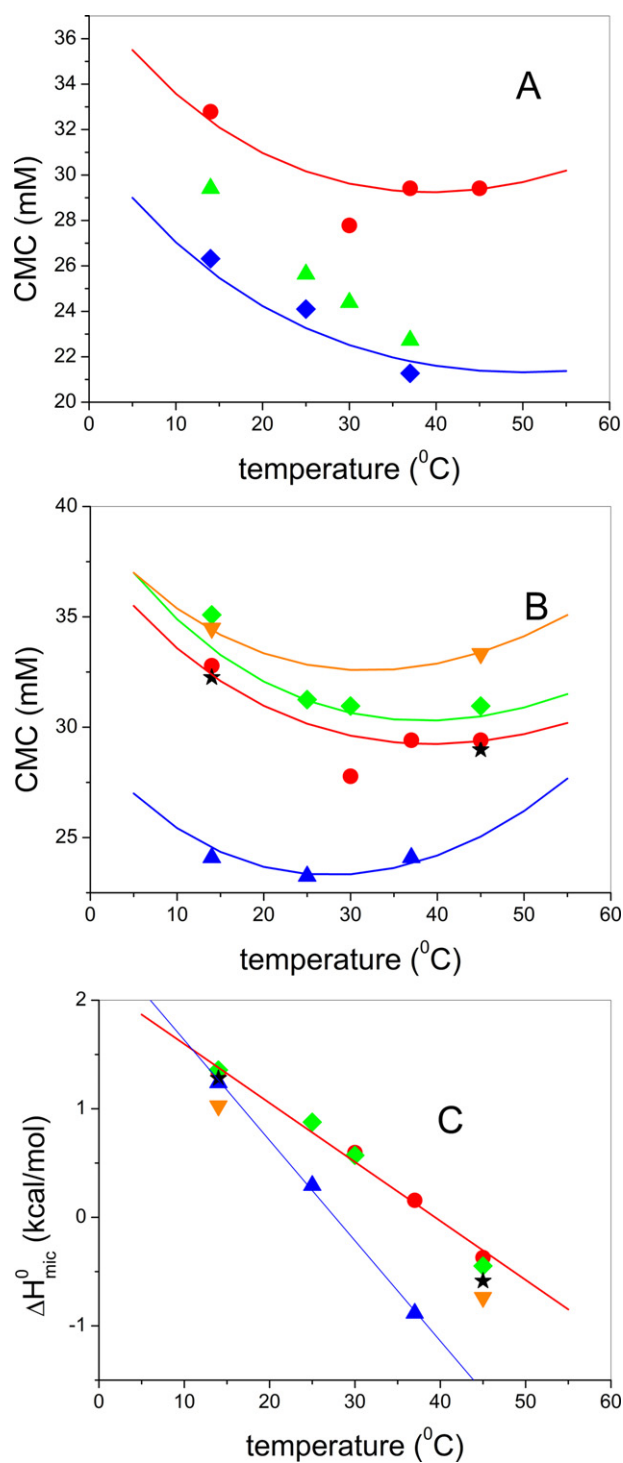
Fig. 1. Critical micellar concentration (CMC) of β-octyl glucoside (β-OG) in the presence of DMSO and rCPT-2 inhibitors 1–4. (A) Influence of DMSO on CMC of β-OG in absence of inhibitors. (♦) β-OG without DMSO, (▲) β-OG + 1% (v/v) DMSO, (●) β-OG + 7.5% (v/v) DMSO. (B) Influence of 7.5% (v/v) DMSO on CMC of β-OG in presence of inhibitors. The inhibitor concentration at the CMC varies between ca. 70–100 μM. (●) β-OG only, (▲) β-OG + inhibitor 1, (▼) β-OG + inhibitor 2, (★) β-OG + inhibitor 3, (♦) β-OG + inhibitor 4. (C) Enthalpy of micelle formation as a function of temperature. (●) β-OG, (▲) β-OG + inhibitor 1, (▼) β-OG + inhibitor 2 (★) β-OG + inhibitor 3, (♦) β-OG + inhibitor 4.

Fig. 2. Calorimetric titration of rCPT-2 with inhibitor 1 at 10 °C. The inhibitor (140 μM) was injected with 25 steps of 10 μl into the calorimetric sample cell containing 11 μM of rCPT-2. (A) Heat flow as a function of time. (B) Reaction enthalpy, δh_i, of inhibitor 1 versus injection number. The solid line corresponds to the theoretical model assuming a 1:1 binding stoichiometry, a reaction enthalpy of $\Delta H^0 = -4.7$ kcal/mol and a binding constant of $K = 8 \times 10^5$ M^{-1}. Buffer composition: 25 mM Tris/HCl pH 8, 150 mM NaCl, 2 mM TCEP, 1% (w/v) β-OG, 1% (v/v) DMSO.
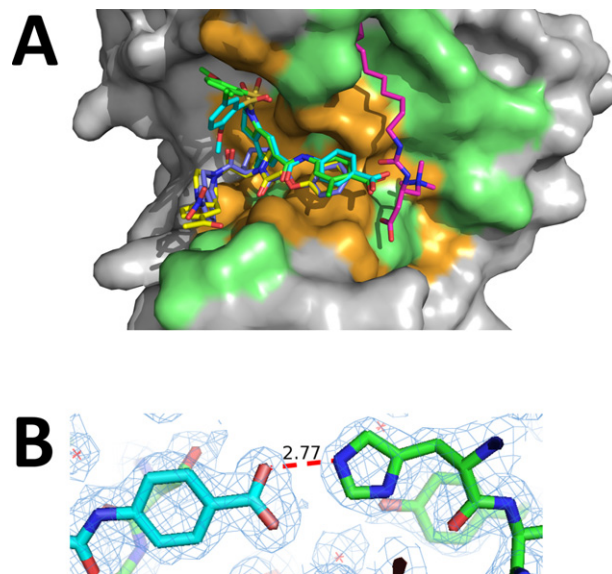
Fig. 3. Structures of rCPT-2 with bound inhibitors 1–4 as determined by X-ray crystallography and computational modeling. (A) Superposition of crystallographic and modeled structures of complexes of rCPT-2 with inhibitors 1 and 2 (blue and yellow, respectively, both modeled based on the crystal structure of a related piperidine class inhibitor, see Supplementary Data), the two isosteric surrogates of inhibitor 3 (cyan and green) and inhibitor 4 (ST1326, magenta). The solvent accessible surface of the carboxy-terminal domain of rCPT-2 (off-white, L441-I656) is shown with hydrophobic residues depicted in green and polar residues shown in orange. The amino terminal domain was removed for clarity. (B) Detail of the complex structure of rCPT-2 (green) with a surrogate of inhibitor 3 (cyan) that shows the interaction of the benzoic acid head group of this inhibitor class with the catalytic residue His372. The minimum distance is 2.8 Å. The final 2FoFc electron density of the structure is shown as gray mesh. (For interpretation of the references to colour in this figure legend, the reader is referred to the web version of this article.)

the PE–cinnamycin complex were thus 10–100 times smaller in the β-OG environment [12] supporting the above conclusion of reduced hydrophobic interactions in the presence of β-OG.
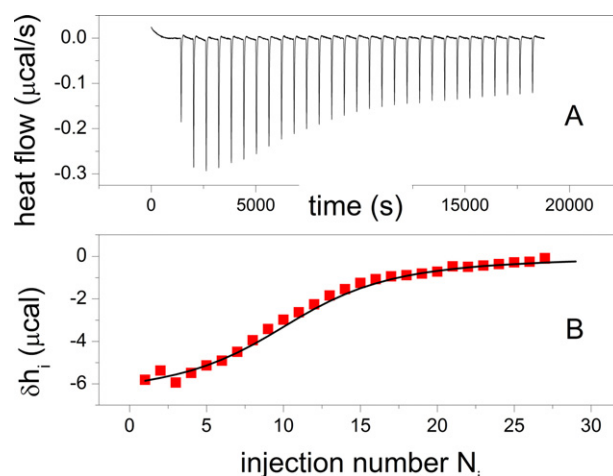
Electrostatic interactions are increased in a non-polar micellar environment because of the lower dielectric constant. Charge neutralization reactions are then characterized by substantial positive heat capacity changes, ΔC_p^0 [30]. Electrostatic effects were revealed by the temperature dependence of the reaction enthalpy, ΔH^0. Inhibitor 3 in Tris/HCl pH 8 buffer showed a linear dependence on temperature with a positive molar heat capacity change of $\Delta C_p^0 = 69$ cal/mol K
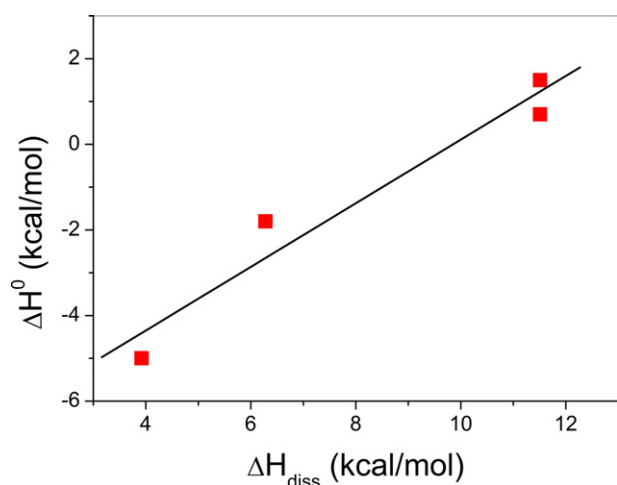
Fig. 4. Proton transfer upon binding of inhibitor 3. The measured binding enthalpy for the interaction of inhibitor 3 with rCPT-2, ΔH_{obs}, is plotted versus the ionization enthalpies of different buffers. Measurements were made in HEPES/NaOH ($\Delta H_{diss} = 3.9$ kcal/mol), Bicine/NaOH ($\Delta H_{diss} = 6.3$ kcal/mol) and Tris/HCl ($\Delta H_{diss} = 11.5$ kcal/mol) at pH 8 and 10 °C. The solid line is the linear regression analysis of the data.
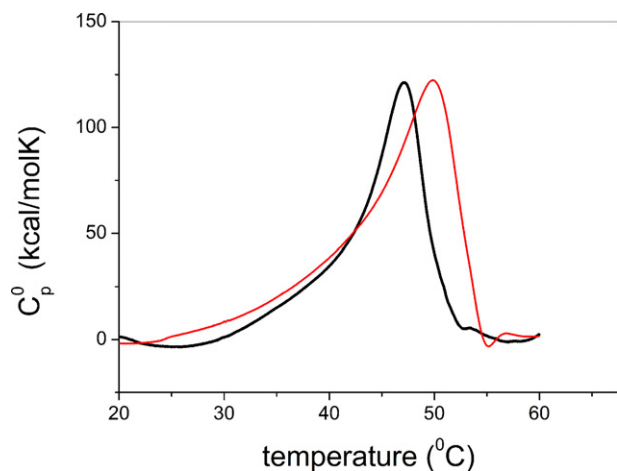

Fig. 5. Experimental DSC scans on rCPT-2 with and without inhibitor 4. Black line: rCPT-2, no inhibitor, Red line: rCPT-2 in the presence of inhibitor 4. rCPT-2 concentration 14 µM, inhibitor 4 concentration 100 µM; buffer conditions as in Fig. 2. (For interpretation of the references to colour in this figure legend, the reader is referred to the web version of this article.)

(Table 3). For the other inhibitors only two temperatures were measured. The ΔC_p^0 values ranged from 314 cal/molK of inhibitor 1 to only 11 cal/mol K of inhibitor 4. The very small ΔC_p^0 of inhibitor 4 indicates that electrostatic interactions ($\Delta C_p^0 > 0$) were almost completely compensated by hydrophobic interactions ($\Delta C_p^0 < 0$).

Table 3 contains the enthalpic and entropic components to the free energy change, ΔG^0. For inhibitors 1 and 2 enthalpy and entropy contribute to equal extent to the binding affinity. For inhibitor 3 the free energy is exclusively enthalpic and the entropy term close to zero if the protonation reaction is neglected. The binding of inhibitor 4 is also enthalpy-driven and shows the most negative ΔH^0 of ~ -10 kcal/mol while the entropy is even counteracting binding. Nevertheless, the binding constants and the free energies of binding of the 4 inhibitors are rather similar in spite of quite different contributions of ΔH^0 and $T\Delta S_0$. The binding of the four inhibitors is thus another example of the enthalpy–entropy compensation effect. The interpretation of ΔH^0 and $T\Delta S_0$ in terms of molecular structures is difficult, but it is common to associate ΔH^0 with van-der-Waals

and electrostatic interactions. However, as these are increased, the molecular structure of the ligand–protein complex rigidifies and the loss in conformational freedom produces a negative $T\Delta S_0$ term which reduces the gain in enthalpy.

In summary, measuring the ligand affinities with ITC has added valuable information on binding modes that can be reconciled with the crystallographic data and docking models. However, the absolute values for binding constants from orthogonal binding assays need to be evaluated regarding the sample composition that is required for each of the methods.

The micromolar K_D-values of inhibitors 1–4 are not sufficient for pharmaceutical purposes and should be reduced to the nanomolar range to increase the potency of the compounds. The challenge therefore is to optimize *both* ΔH^0 and $T\Delta S_0$. Calorimetric measurements will be helpful in verifying different synthetic concepts.

Supplementary Material

Supplementary material associated with this article can be found, in the online version, at doi:10.1016/j.fob.2013.04.003.

References

[1] de Vries Y., Arvidson D.N., Waterham H.R., Cregg J.M., Woldegiorgis G. (1997) Functional characterization of mitochondrial carnitine palmitoyltransferases I and II expressed in the yeast *Pichia pastoris*. Biochemistry 36, 5285–5292.
[2] Bonnefont J.P., Djouadi F., Prip-Buus C., Gobin S., Munnich A., Bastin J. (2004) Carnitine palmitoyltransferases 1 and 2: biochemical, molecular and medical aspects. Mol. Aspects Med. 25, 495–520.
[3] Zammit V.A. (1999) Carnitine acyltransferases: functional significance of subcellular distribution and membrane topology. Prog. Lipid Res. 38, 199–224.
[4] Foster D.W. (2004) The role of the carnitine system in human metabolism. Ann. N.Y. Acad. Sci. 1033, 1–16.
[5] Deschauer M., Wieser T., Zierz S. (2005) Muscle carnitine palmitoyltransferase II deficiency: clinical and molecular genetic features and diagnostic aspects. Arch. Neurol. 62, 37–41.
[6] Ceccarelli S.M., Chomienne O., Gubler M., Arduini A. (2011) Carnitine palmitoyl-transferase (CPT) modulators: a medicinal chemistry perspective on 35 years of research. J. Med. Chem. 54, 3109–3152.
[7] Rufer A.C., Lomize A., Benz J., Chomienne O., Thoma R., Hennig M. (2007) Carnitine palmitoyltransferase 2: analysis of membrane association and complex structure with a substrate analog. FEBS Lett. 581, 3247–3252.
[8] Rufer A.C. (2006) The crystal structure of carnitine palmitoyltransferase 2 and implications for diabetes treatment. Structure 14, 713–723.
[9] Nic á Bhaird N., Kumaravel G., Gandour R.D., Krueger M.J., Ramsay R.R. (1993) Comparison of the active sites of the purified carnitine acyltransferases from peroxisomes and mitochondria by using a reaction-intermediate analogue. Biochem. J. 294(Pt. 3), 645–651.
[10] Hsiao Y.S., Jogl G., Esser V., Tong L. (2006) Crystal structure of rat carnitine palmitoyltransferase II (CPT-II). Biochem. Biophys. Res. Commun. 346, 974–980.
[11] Machaidze G., Ziegler A., Seelig J. (2002) Specific binding of Ro 09–0198 (cinnamycin) to phosphatidylethanolamine: a thermodynamic analysis. Biochemistry 41, 1965–1971.
[12] Machaidze G., Seelig J. (2003) Specific binding of cinnamycin (Ro 09–0198) to phosphatidylethanolamine. Comparison between micellar and membrane environments. Biochemistry 42, 12570–12576.
[13] Beck A., Li-Blatter X., Seelig A., Seelig J. (2010) On the interaction of ionic detergents with lipid membranes. Thermodynamic comparison of n-alkyl-+N(CH) and n-alkyl-SO. J. Phys. Chem. B 114, 15862–15871.
[14] Majhi P.R., Blume A. (2001) Thermodynamic characterization of temperature-induced micellization and demicellization of detergents studied by differential scanning calorimetry. Langmuir 17, 3844–3851.

[15] Paula S., Sus W., Tuchtenhagen J., Blume A. (1995) Thermodynamics of micelle formation as a function of temperature – a high-sensitivity titration calorimetry study. J. Phys. Chem. 99, 11742–11751.

[16] Birdsall B., King R.W., Wheeler M.R., Lewis C.A. Jr., Goode S.R., Dunlap R.B. et al. (1983) Correction for light absorption in fluorescence studies of protein–ligand interactions. Anal. Biochem. 132, 353–361.

[17] Eftink M.R. (1997) Fluorescence methods for studying equilibrium macromolecule-ligand interactions. Methods Enzymol. 278, 221–257.

[18] Bieber L.L., Fiol C. (1986) Purification and assay of carnitine acyltransferases. Methods Enzymol. 123, 276–284.

[19] Fiol C.J., Bieber L.L. (1988) Effects of octylglucoside and triton X-100 on the kinetics and specificity of carnitine palmitoyltransferase. Lipids 23, 120–125.

[20] Bieber L.L. (1988) Carnitine. Annu. Rev. Biochem. 57, 261–283.

[21] Johnson T.M., Mann W.R., Dragland C.J., Anderson R.C., Nemecek G.M., Bell P.A. (1995) Over-expression and characterization of active recombinant rat liver carnitine palmitoyltransferase II using baculovirus. Biochem. J. 309(Pt. 2), 689–693.

[22] Allen F.H. (2002) The Cambridge structural database: a quarter of a million crystal structures and rising. Acta Crystallogr. Sect. B Struct. Sci. B 58, 380–388.

[23] DeGrip W.J., Bovee-Geurts P.H.M. (1979) Synthesis and properties of alkylglucosides with mild detergent action – improved synthesis and purification of beta-1-octyl-glucose, beta-1-nonyl-glucose and beta-1-decyl-glucose – synthesis of beta-1-undecylglucose and beta-1-dodecylmaltose. Chem. Phys. Lipids 23, 321–335.

[24] Milletti F., Storchi L., Sforna G., Cruciani G. (2007) New and original pKa prediction method using grid molecular interaction fields. J. Chem. Inf. Model 47, 2172–2181.

[25] Milletti F., Storchi L., Goracci L., Bendels S., Wagner B., Kansy M. et al. (2010) Extending pKa prediction accuracy: high-throughput pKa measurements to understand pKa modulation of new chemical series. Eur. J. Med. Chem. 45, 4270–4279.

[26] Goldberg R.N., Kishore N., Lennen R.M. (2002) Thermodynamic quantities for the ionization reactions of buffers. J. Phys. Chem. Ref. Data 31, 231–370.

[27] Forneris F., Mattevi A. (2008) Enzymes without borders: mobilizing substrates, delivering products. Science 321, 213–216.

[28] Sikora C.W., Turner R.J. (2005) Investigation of ligand binding to the multidrug resistance protein EmrE by isothermal titration calorimetry. Biophys. J. 88, 475–482.

[29] Housden N.G., Wojdyla J.A., Korczynska J., Grishkovskaya I., Kirkpatrick N., Brzozowski A.M. et al. (2010) Directed epitope delivery across the *Escherichia coli* outer membrane through the porin OmpF. Proc. Natl. Acad. Sci. U.S.A. 107, 21412–21417.

[30] Lewis G.N., Randall M., Pitzer K.S., Brewer L. (1961) McGraw-Hill, New York.